Core Heating Scaling for Fast Ignition Experiment FIREX-I

T. Johzaki 1), H. Nagatomo 1), A. Sunahara 2), H.-B. Cai 3), H. Sakagami 4), Y. Nakao 5), K. Mima 1), H. Nakamura 1), S. Fujioka 1), H. Shiraga 1), H. Azechi 1), and FIREX project group

1) Institute of Laser Engineering, Osaka University, Suita, Japan
2) Institute for Laser Technology, Suita, Japan
3) Institute for Applied Physics and Computational Mathematics, Beijing, China
4) National Institute for Fusion Science, Toki, Japan
5) Department of Applied Quantum Physics and Nuclear Engineering, Kyushu University, Fukuoka, Japan

E-mail contact of main author: tjohzaki@ile.osaka-u.ac.jp

Abstract. The effect of pre-plasma on core heating in cone-guiding fast ignition is evaluated by two-dimensional Particle in Cell (PIC) and Fokker-Planck (FP) simulations. If the long-scale pre-plasma exists in the cone, the generated fast electron energy becomes too high for effective core heating. As the result, the energy coupling from laser to core $\eta_{L\rightarrow core}$ is reduced by 80% compared with the case without pre-plasma. Even for the case without pre-plasma, $\eta_{L\rightarrow core}$ obtained in the simulation is smaller than that required for 5keV heating in FIREX-I. In order to enhance $\eta_{L\rightarrow core}$, we propose a new target design (extended double cone for fast electron guiding to imploded core, pointed low-Z cone tip for reducing the collisional effects on fast electron transport and for reducing its effect on implosion, and thin foil pre-pulse absorber) and evaluate its performance by PIC, FP and radiation-hydro simulations.

1. Introduction

In Institute of Laser Engineering (ILE), Osaka University, a 4-beam bundled new ultra-intense high-energy laser LFEX (Laser for Fast-ignition Experiment) has been constructed, and FIREX-I (Fast-Ignition Realization Experiment Project, Phase-I) [1] has been started. The final goal of FIREX-I is demonstration of core heating up to 5keV using 10kJ heating laser. Previously, we have carried out the integrated simulations [2], which reproduced the core heating properties of the PW experiments [3] and showed the importance of pre-plasma in core heating performance. In the present paper, on the basis of the integrated simulations, we analyze the first integrated experiments using LFEX laser and propose the new target design for enhancing the core heating efficiency and achieving the final goal of FIREX-I.

2. Integrated Experiments

The first integrated experiments using LFEX laser have been done, where the LFEX laser was operated with one-beam and low-energy mode. In Fig.1(a), the observed neutron yields are plotted as a function of the heating laser energy for difference laser pulse duration (duration of 5ps;▼ and 1ps;▲). About 30-foled enhancement in neutron yield was achieved by the heating laser irradiation. However, this enhancement is smaller than that in the previous experiments using PW laser, where the heating laser energy is comparable to the present experiments (the results are shown by solid circles in Fig.1(a); ~1000-fold enhancement was observed). Compared to the results of two-dimensional (2D) core heating simulations [4], where the energy coupling of heating laser to compressed core $\eta_{L\rightarrow core}$ was assumed by 3 ~ 20% (lines in Fig.1(a)), $\eta_{L\rightarrow core}$ ~20% was expected in the PW experiment, but only $\eta_{L\rightarrow core}$ = 3~5% at the present LFEX experiments. One reason for the low energy coupling is un-sufficient optimization of heating pulse, especially, existence of relatively high-level pre-

pulse. The pre-pulse generates the long-scale pre-formed low dense plasma (pre-plasma) inside the cone, which results in leading the fast electron generation point away from the core and in generating very energetic fast electrons not contributing the core heating.

The DD-neutron weighted ion temperature $<T_i>_{DD}$ evaluated by the 2D core heating simulations are plotted in Fig.1(b) as a function of heating laser. To achieve $<T_i>_{DD}$ ~5keV with full-spec LFEX laser (10kJ laser energy), $\eta_{L\rightarrow core}$ ~15% is required. To enhance the energy coupling than the present experiments, reduction of pre-pulse level is indispensable.

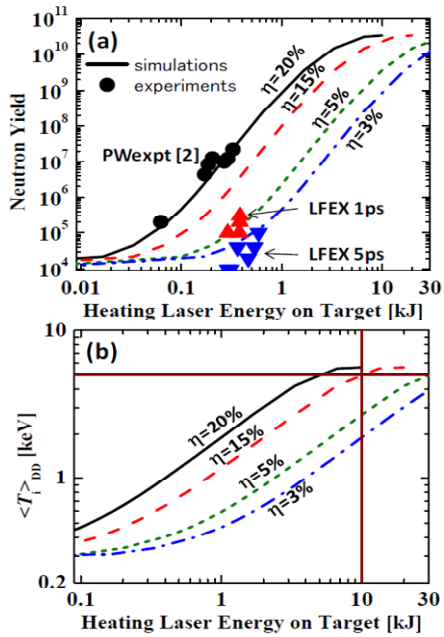

FIG.1. (a) neutron yields and (b) averaged core temperature $<T_i>_{DD}$ as a function of heating laser energy.

3. Integrated Simulations for Evaluation of Pre-Plasma Effects

To evaluate the pre-plasma effects on core heating in cone-guiding fast ignition, we carried out the integrated simulations, where the fast electron generation at the laser-cone interactions is simulated with a 2D Particle in Cell (PIC) code, and then the core heating process is simulated with 2D Fokker-Planck (FP) code using the fast electron profiles obtained at the PIC simulations.

3. 1 Fast Electron Generation

The laser-cone interactions were simulated with a 2D PIC code ASCENT [5]. Figure 2 shows an initial density profile of cone. The Au cone (Z=40, electron density of $100n_c$,n_c is laser critical density, 30 degree open angle, 12μm tip width, 5μm tip thickness, 8μm side wall thickness) is surrounded by imploded CD plasma ($50n_c$, Z=3.5). We carried out the simulations for the two cases. One is the small pre-plasma case where a exponential-profile pre-plasma with scale length of λ_p = 1μm is attached on the inner surface of the cone tip from $100n_c$ density down to $0.1n_c$. The other is the larger pre-plasma case, where in addition to λ_p = 1μm small pre-plasma, a λ_p = 10μm long-scale pre-plasma is attached from $5n_c$ point. In the following, the former (the latter) is called as the case without (with) pre-plasma. The *p*-polarized laser pulse with λ_L = 1.06 μm wavelength and 3×10^{19} W/cm^2 intensity irradiates the cone from the left boundary. The transverse intensity profile is the Gaussian with a spot size of 16.5μm FWHM. The laser rises in $10T_0$, where T_0 is the laser period. After that the laser amplitude is kept constant during 1ps, and then is dropped to zero in $10T_0$. A typical simulation time is $450T_0$, which corresponds to about 1.6 ps for λ_L = 1.06 μm. The generated fast electrons are observed at the tip (x = 42μm).

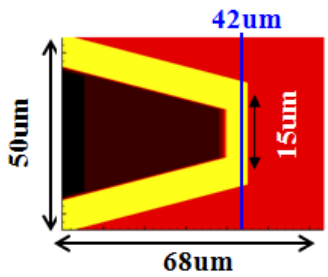

FIG. 2 Initial density profile of cone.

The spatial profiles of laser fields, electron energy density and longitudinal momentum distribution at 240 T_0 are shown in Fig.3. For the case without pre-plasma, the laser light is reflected at the wall and then focused at the tip. The fast electrons are mainly generated at the tip. Contrary to this, for the case with pre-plasma, the laser light is strongly focused and

breaks into some filaments during the propagation in the pre-plasma. The fast electrons are mainly generated in the pre-plasma region and their momenta are much higher than those for the case without pre-plasma.

The fast electron beam energy and the energy spectrum evaluated at the end of tip (x=42μm) are plotted in Fig.4. The spectrum is evaluated in the region of 15μm width (-7.5 μm < y < 7.5 μm) which is slightly wider than the inner tip size. In both cases, the beam energy is peaked at the centre of the tip. For the case with pre-plasma, the fast electron generation point is away from the tip, so the number of electrons escaping through the side wall is larger. Thus the beam energy at the tip becomes smaller. In addition, due to the laser-plasma interactions in the sub critical density region, the high energy tail is formed in the energy spectrum and then the number of low energy electron (energy E < 10MeV) which mainly contributes to core heating is decreased. The beam divergence observed at the tip is not so different between two cases; ~ 80 degree full angle. The fast electron beam energy observed at tip in the 15μm width is summarized in Table I. The energy conversion ratio from laser to fast electrons $\eta_{L\rightarrow fe}$ is 48% for the case without pre-plasma. The value of $\eta_{L\rightarrow fe}$ is reduced by 24% for the case with pre-plasma. Moreover, the reduction in low-energy electrons due to pre-plasma is serious. Most of the beam energy is carried out by the high energy electrons (E > 10MeV). The beam energy carried by the low energy electrons (E < 10MeV) becomes about 1/4 of that for the case without pre-plasma.

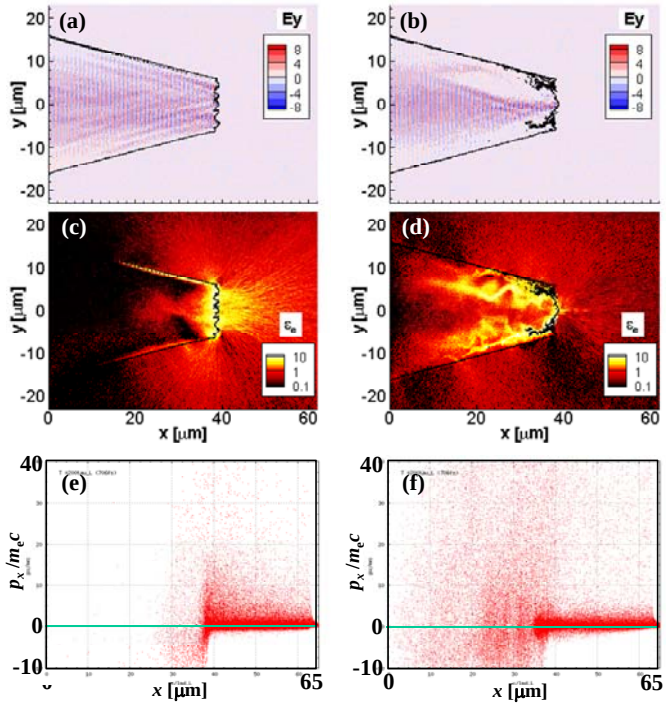

FIG.3 Spatial profiles of laser electric fields E_y (a) and (b), fast electron energy density ε_e (c) and (d), and longitudinal momentum (p_x) at 240T_0 (1ps). The longitudinal momentum is observed in the region of 5μm width (-.25μm < y < 2.5μm). The left and right lines show the cases without and with pre-plasma. The electric fields and energy density are normalized by $m_e\omega_0c/e$ and $m_ec^2n_c$, respectively, where m_e, ω_0, c and e are electron rest mass, laser frequency, speed of light and elementary charge.

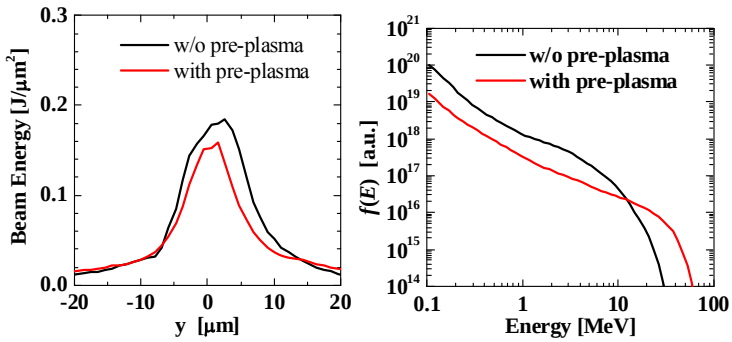

FIG.4. Time-integrated profiles of fast electron observed at x=42μm.The left one is the transverse distribution of fast electron beam energy, and the right one is the energy spectrum observed in the 15μm width region.

Table.I Summary of fast electron profiles observed at the tip within the 15μm width region

	W/o pre-plasma	With pre-plasma	Ratio*
Total beam energy	2.05J/μm (48%#)	1.57J/μm (36%#)	-24%
Fraction			
E < 2MeV	0.56J/μm (13%#)	0.12J/μm (3%#)	-78%
2MeV < E < 10MeV	1.16J/μm (26%#)	0.34J/μm (8%#)	-71%
E > 10MeV	0.34J/μm (8%#)	1.10J/μm (25%#)	+230%

Energy conversion ratio of laser to fast electrons.
* Reduction(-) or enhancement (+) in the beam energy due to pre-plasma.

3. 2 Core Heating

The core heating simulations were carried out with FP and hydro hybrid code FIBMET [6] using the time- and transverse-position- dependent energy and angular distributions of fast electron observed at the tip in above PIC simulations as the fast electron beam sources. An uniformly compressed CD spherical plasma (0.15g/cm^2 areal density, the Gaussian density profile with 100g/cm^3 peak density and 28.4μm FWHM, and 300eV uniform temperature) is assumed as the imploded core. The fast electron beam is injected at 60μm away from the core centre. In the PIC simulations, due to the limitation of the computational resource, we assumed 12μm inner tip width, which is smaller than the actual cone tip size (at the previous experiments, the inner tip width was 40μm). So in the heating simulations, we used the PIC simulation results by simply widening the beam size by 3.3.

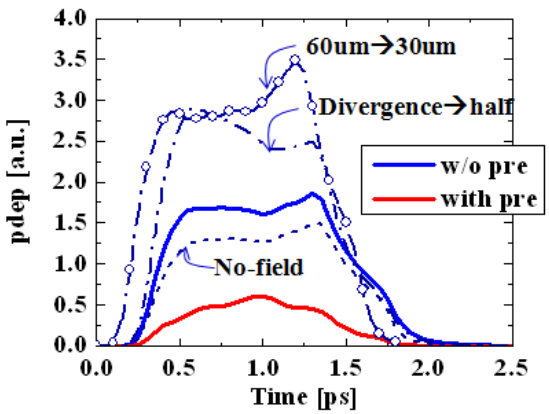

FIG.5. Temporal evolution of core heating rates. The solid lines are for the cases without pre-plasma (blue) and with pre-plasma (red). For the case without pre-plasma, we also plotted the results in the cases when (a) electromagnetic field is turned off (broken line), (b) beam divergence is made half (dash-dot line), and (c) beam injection point is moved close to the core (30mm away from the core centre) (marked line).

The obtained core heating rates are plotted in Fig.5 as a function of time. The energy coupling efficiency and resultant core temperature $<T_i>_{DD}$ are summarized in Table.II. It is found that for the case with pre-plasma, the core heating rate is significantly decreased. This is due to the reduction of low energy component in the fast electron beam. The value of $\eta_{L\rightarrow core}$ becomes ~1/5 compared to the case without pre-plasma. This reduction rate is comparable to the experimental results shown in section 2. For the efficient core heating, thus, the elimination of pre-plasma is essential. The beam collimation effect due to the resistive field has been reported in previous works [7-9]. However, because of the large beam divergence at the cone tip, this effect is not so pronounced (comparison between blue solid and blue broken lines). Even for the case without pre-plasma, $\eta_{L\rightarrow core}$ is still lower than that required for 5keV heating ($\eta_{L\rightarrow core}$ ~15%). The way to enhance the energy coupling from fast electron to the core is (a) making the beam divergence smaller (blue dash-dot line) or (b) putting the tip close to the core or guiding the beam close to the core (blue line with open circles).

Table.II Summary of energy coupling efficiency and temperature enhancement.

Simulation condition				$\eta_{L\to fe}$[%] (energy coupling of laser to fast electron)	$\eta_{fe\to core}$[%] (energy coupling of fast electron to core)	$\eta_{L\to core}$[%] (total coupling; laser to core)	$<T_i>_{DD}$ [keV]
Pre-plasma	Injection point from core centre [μm]	Electro-magnetic field	θ_{beam}				
w/o	60	on	PIC	48	16	7.5	0.75
with	60	on	PIC	36(-24%)	4.7(-71%)	1.7(-78%)	0.35
w/o	60	**off**	PIC	48	12(-23%)	5.8(-23%)	0.47
w/o	60	on	**1/2 PIC**	48	25(+57%)	12(+57%)	0.77
w/o	**30**	on	PIC	48	29(+80%)	14(+80%)	0.85

The values in () are the reduction [-] (or the enhancement [+]) rates compared to the reference case (the first line). "PIC" ("1/2PIC") in θ_{beam} columns means that as the source divergence in FP simulation, the fast electron beam divergence obtained at the PIC simulations is used without change (by reducing it to half).

4. New Target Design for Enhancing Core Heating Efficiency

To enhance the core heating efficiency, we proposed a new target design (Fig.6). This concept is based on the double cone [5, 10]. The original idea of double cone is to confine the fast electrons to escape from the cone side wall by electrostatic and quasi-static magnetic fields foamed in the vacuum gap region. In the new concept, we extend the cone tip and vacuum gap in order to guide the fast electrons close to the core. (We call it "extended double cone".) In addition, by changing the diameter of the end of tip, the beam spot size can be controlled. In future ignition experiments, the laser energy becomes ~100kJ. If such a high energy laser is focused in a small spot (~30μmϕ) with the duration of ~10ps, the intensity reaches ~10^{21}W/cm^2, which results in generating very high energy fast electrons and reducing the heating efficiency. Using this extended double cone, we can reduce the laser intensity by pulling the tip inner surface away from the core (which means widening the interaction surface area). In this case, fast electrons travel long distance in the tip, so that low-Z material is used as the tip material to reduce the collisional effects [9, 11]. The shape of the tip is changed from flat one to pointed one to reduce its effect on the implosion. To reduce the pre-pulse generating the pre-plasma, a very thin foil (0.05 ~ 0.1μm CH or diamond-like carbon (DLC)) is attached at the entrance of the cone as a pre-pulse absorber [12]. To suppress the Rayleigh-Taylor instability, a Br doped shell [13] is adopted. The cone outer surface is coated with CH thin layer to prevent the cone material (here Au) from being heated and then to tamp the cone material ablation [14]. In the following sub sections, we present the effects of (1) extended double cone, (2) pointed low-Z tip and (3) thin foil pre-pulse absorber.

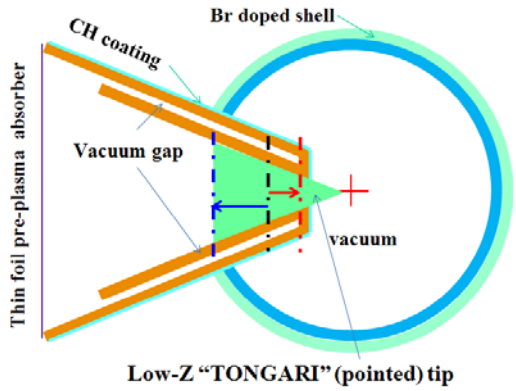

FIG.6. Schematic view of new target design. The black line shows the normal tip inner surface position, the red line shows the extended tip-end position to guide the fast electron close to the core and the blue line shows the tip inner position pulled away from the core to reduce the laser intensity and then soften fast electron spectrum.

4.1 Extended Double Cone

The performance of extended double cone was evaluated with 2D PIC and FP simulations. Figure 7 shows an initial density profile of extended double cone for 2D PIC simulation. Compared with the single cone (Sec.3.1) the 3μm width vacuum gap is introduced in the side wall and the tip & gap are extended 20μm to the core direction. The distance between two gaps at the end of tip is about 8μm. The other parameters (density, pre-plasma condition and so on) and the laser condition are the same as those in Sec.3.1.

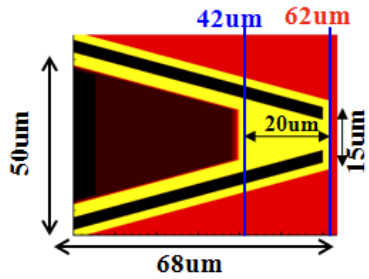

FIG.7. Initial density profile of extended double cone

The spatial profiles of laser field, quasi-static magnetic field and fast electron energy density at $280T_0$ are shown in Fig.8. In the extended gap region, the surface return current is driven by the fast electrons generated by laser-plasma interactions, which forms the quasi static magnetic fields. Its strength is ~300MG and the width of gap is 3μm. The fields are strong enough to confine the fast electron with energy of < 10MeV since the Larmor radius of 10MeV electron is 1.2μm for 300MG field. Thus, the fast electrons are trapped in the tip region and released from the "B-field open gate" between two gaps at the end of tip. The transverse profile of beam energy and energy spectrum observed at the end of tip (x=62μm) are shown in Fig.9, together with the single cone results observed at the same position. In the single cone case, compared to Fig.4 left, the fast electron beam is strongly diverged in the transverse direction after 20μm propagation from the tip. Contrary to this, for the extended cone case, the fast electron beam is successfully guided to the position close to the core by the extended gap effects.

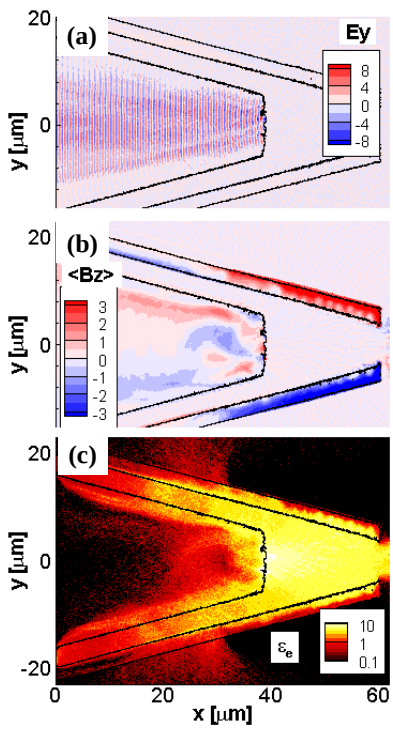

FIG.8. Spatial profiles of (a) laser field, (b) quasi-static magnetic fields and (c) fast electron energy density at $280T_0$ for the extended double cone without pre-plasma. The quasi-static magnetic field is normalized by $m_e\omega_0 c/e$.

Using the fast electron profiles obtained at the PIC simulation, we carried out the core heating simulation. The core profile and the beam injection condition are the same as that in Sec.3.2 except for the beam injection point. In view of tip extension, we set the beam injection point close to core (injection at 30μm away from the core centre). The energy coupling efficiency and resultant core temperature $\langle T_i \rangle_{DD}$ are summarized in Table.III. In the extended cone, some of

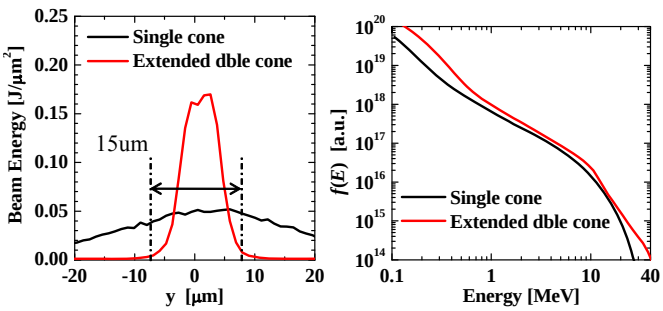

FIG.9. Transverse profiles of fast electron beam energy (left) and energy spectrum (right) observed at x = 62μm. The spectrum is evaluated by counting the fast electron in the 15μm width region.

fast electrons trapped by magnetic field around the tip region escape from the side wall after scattering by magnetic fields, so the value of $\eta_{L\rightarrow fe}$ observed at the tip end (x = 62μm for the extended cone) in the 15μm width region is smaller than that for the single cone (observed at x=42μm). However, due to the extended gap effects, the fast electrons are released from the end of extended tip located close to the core and the beam is collimated at the tip end. So $\eta_{fe\rightarrow core}$ is significantly increased compared with the single cone case. Thus, the total coupling $\eta_{L\rightarrow core}$ for the extended double cone becomes ~ 3 times larger than that for the single cone. Even if the extended double cone is used, however, the reduction in heating efficiency due to the pre-plasma cannot be overcome.

Table.III Summary of energy coupling efficiency and temperature enhancement.

Simulation condition			$\eta_{L\rightarrow fe}$[%]*	$\eta_{fe\rightarrow core}$[%]	$\eta_{L\rightarrow core}$[%]	$<T_i>_{DD}$ [keV]
Cone type	Pre-plasma	Injection point [μm]				
Single	w/o	60	48 (18)	16	7.5	0.75
Single	with	60	36 (14)	4.7	1.7	0.35
Extended double	w/o	30	31	62	19	1.27
Extended double	with	30	20	28	5.5	0.70

* $\eta_{L\rightarrow fe}$ is evaluated at the tip end in the 15μm width region (*i.e.*, at x =42 μm for the single cone case and x = 62 μm for the extended double cone case). The values in () are $\eta_{L\rightarrow fe}$ observed at x=62μm point in 15μm width for the single cone.

4.2 Pointed Low-Z Tip

We evaluated the implosion performance of a pointed low-Z tip by radiation hydro simulations with PINOCO [14]. The CD shell target (250 μm shell inner radius, 6.8μm shell thickness) with 45 degree open-angle Au cone is irradiated with 2.0kJ Gaussian laser pulse with 0.53μm wavelength. The simulations are carried out for the two cases; one is normal tip (flat Au tip) located at 50μm from the shell centre, the other is the pointed CH tip where the tip end is located at the shell centre. In Fig.10, the spatial profiles of density and temperature around the core are shown for the two cases at the two different moments. It is found that the pointed low-Z tip does not affect the implosion performance. In both cases, the maximum compression is achieved at 2.74ns and the obtained areal density is 0.63g/cm^2. The timing when the shock from the core reaches the tip inner surface becomes ~30ps later, which is preferable to the core heating.

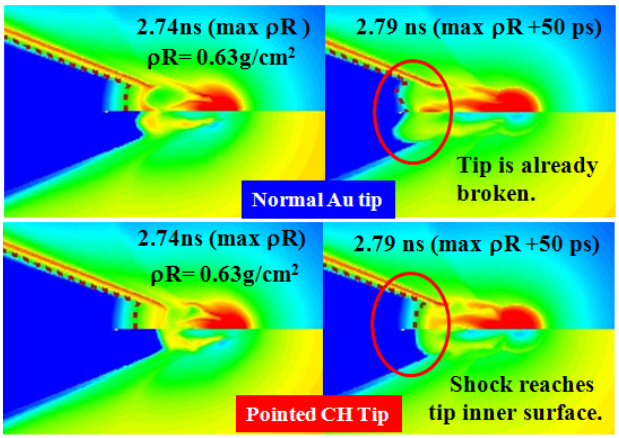

FIG. 10. Spatial profiles of density (upper half) and temperature (lower half) around the core. The upper two figures are for the normal Au tip case and the lower two figures for the pointed CH tip.

4.3 Thin Foil Pre-Plasma Absorber

The thin foil placed at the cone entrance becomes plasma and starts to expand by absorbing the pre-pulse of the heating laser. The density of the expanded plasma should be low enough not to affect the propagation of main pulse of the heating laser. We simulated the dynamics of

this irradiated CH foil to optimize the thickness by 2D radiation-hydro code Star2D [15]. The 1.06μm wavelength laser having a flat top in time and the Gaussian profile in space with 100 μm (FWHM) irradiates 0.05~ 0.1μm thickness CH foils with intensity of 10^{11}~10^{12}W/cm^2 and normally incident. Figure 11 shows a spatial profile of the electron number density n_e at 1.8ns. The density of the CH plasma becomes low enough not to absorb the 1.06 μm laser (n_e <10^{20} cm^{-3} along the laser axis), and the plasma expands 1mm scale along the laser axis. At this timing, the laser absorption fraction is 0.15, and 85% of the laser power can penetrate the CH plasma. Consequently, the almost power of the main pulse is expected to be able to propagate the expanded plasma without any significant absorption. From simulations, 0.1μm thickness CH foil can be used for the pre-pulse absorber to suppress the pre-pulse with the intensity of 3x10^{11}W/cm^2 and 1.8ns duration.

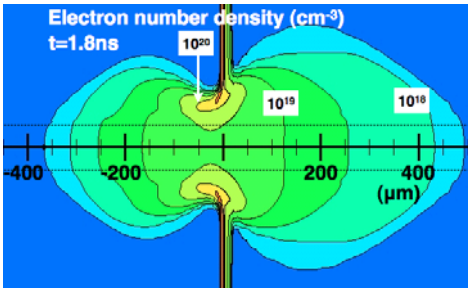

FIG.11. Electron number density n_e(cm^{-3}) at 1.8ns. Foil thickness is 0.1μm. Laser intensity is 3x10^{11}W/cm^2. Laser spot size is 100μm (FWHM) is shown by dotted line.

5. Summary

It was found from the 2D PIC and FP simulations for core heating in cone-guiding fast ignition that the energy coupling from laser to core $\eta_{L\rightarrow core}$ is reduced by 80% due to the long-scale (10μm) pre-plasma in the cone since the fast electron energy becomes too high. Even for the case without pre-plasma, $\eta_{L\rightarrow core}$ is not high enough to achieve 5keV heating in FIREX-I. In order to enhance $\eta_{L\rightarrow core}$, we proposed a new target design (extended double cone, pointed low-Z cone tip, and thin foil pre-pulse absorber) and showed its performance by PIC, FP and radiation-hydro simulations.

References

[1] H. Azechi, *et al*., 2006 *Plasma Phys. Control. Fusion* **47** B267 (2006).
[2] T. Johzaki, et al., 2007 *Laser Part. Beams* **25** 621 (2007).
[3] R. Kodama, *et al*., 2002 *Nature* **418** 933 (2002).
[4] T. Johzaki, e*t al.,* 2008 *Phys. Plasmas* **15** 062702 (2008).
[5] H.-B. Cai, *et al.,* Phys. Rev. Lett.**102**, 245001 (2009); *Phys. Plasmas* **17** 023106 (2010).
[6] T. Johzaki, *et al., J. Phys. IV* **133**, 358 (2006), T. Yokota, *et al., Phys. Plasmas* **13**, 022702 (2006).
[7] J. J. Honrubia, *et al., Nucl. Fusion* **46**, L25 (2006).
[8] T. Johzaki, *et al., J. Phys.: Conf. Ser.* **112**, 022054 (2008).
[9] T. Jozaki, *et al., Phys. Plasmas* **16**, 062706 (2009).
[10] T. Nakamura, *et al., Phys. Plasmas* **14**, 103105 (2007).
[11] T. Johzaki, *et al., Plasma Phys. Control. Fusion* **51**, 014002 (2009).
[12] K. Kinoshita, *et al., App. Phys. Lett.* **84**, 4623 (2004)
[13] S. Fujioka, *et al., Phys. Rev. Lett.* **92**, 195001 (2004).
[14] H. Nagatomo, *et al., Nucl. Fusion* **49**, 075028 (2009).
[15] A. Sunahara, *et al., J. Phys.: Conf. Ser.* **112**, 042048 (2008).